High-Order Quasi-Helmholtz Projectors: Definition, Analyses, Algorithms

High-Order Quasi-Helmholtz Projectors: Definition, Analyses, Algorithms

Johann Bourhis, *Graduate Student Member, IEEE*, Adrien Merlini, *Senior Member, IEEE*, and Francesco P. Andriulli, *Fellow, IEEE*

***Abstract*— The accuracy of the electric field integral equation (EFIE) can be substantially improved using high-order discretizations. However, this equation suffers from ill-conditioning and deleterious numerical effects in the low-frequency regime, often jeopardizing its solution. This can be fixed using quasi-Helmholtz decompositions, in which the source and testing elements are separated into their solenoidal and nonsolenoidal contributions, and then rescaled to avoid both the low-frequency conditioning breakdown and the loss of numerical accuracy. However, standard quasi-Helmholtz decompositions require handling discretized differential operators that often worsen the mesh refinement ill-conditioning and require the finding of the topological cycles of the geometry, which can be expensive when modeling complex scatterers, especially in high-order. This article solves these drawbacks by presenting the first extension of the quasi-Helmholtz projectors to high-order discretizations and their application to the stabilization of the EFIE when discretized with high-order basis functions. Our strategy will not require the identification of the cycles and will provide constant condition numbers for decreasing frequencies. Theoretical considerations will be accompanied by numerical results showing the effectiveness of our method in complex scenarios.**

***Index Terms*— Boundary element method (BEM), electric field integral equation (EFIE), high-order, low-frequency, preconditioning, quasi-Helmholtz projectors.**

I. Introduction

MODELING and simulation of electromagnetic scattering from perfectly electrically conducting (PEC) objects can be effectively performed using surface integral equations [1], [2]. Among these formulations, the electric field integral equation (EFIE) is one of the most widely used. This equation is usually solved via the boundary element method (BEM) [3] by approximating the current as a combination of basis functions with a finite support defined on a surface mesh of the object. The accuracy of the method consequently depends on the ability of the mesh and basis functions to, respectively, describe the surface and the current's functional space. Very often, zeroth-order basis functions such as the Rao–Wilton–Glisson (RWG) functions are used with flat triangular cells [4]. Thus, mesh density and functional space discretization are usually increased simultaneously by refining the mesh, which leads to a higher number of cells and basis functions.

Alternatively, high-order mesh and functional space discretizations [5], [6] can be used to improve the accuracy without necessarily increasing the mesh density. High-order basis functions also provide a faster convergence to the physical solution when refining the mesh [7], [8]. Nevertheless, despite the use of a more accurate framework, the EFIE suffers from ill-conditioning and loss of significant digits at low frequency [9].

The stabilization of the EFIE using quasi-Helmholtz decomposition [10], [11], [12], [13] is well-known, even in the high-order case [14], [15]. It consists in a change in basis that allows to reorganize the system into solenoidal and nonsolenoidal contributions and to rescale them appropriately to cure the problematic behavior of the EFIE at low frequency. However, the construction of the solenoidal basis functions can be burdensome because it requires the identification of the global cycles, a task that might be challenging when modeling complex geometries [9]. Other strategies leading to a low-frequency stabilized system are also possible, such as the generalized Debye-source-based EFIE [16], [17], where the EFIE is directly discretized with solenoidal and irrotational basis functions, or such as the augmented EFIE [18], where the mixed potential form of the EFIE is used by including the charge as an additional unknown.

More recently, the method of the quasi-Helmholtz projectors has been developed for the stabilization of the EFIE discretized with RWG functions [9]. The method generates orthogonal projectors over the solenoidal and nonsolenoidal subspaces from the computation of the Star matrix, without having to explicitly identify the cycles. They are subsequently used to separate and to rescale the different contributions of the EFIE, without further degrading the condition number when increasing the mesh density [9].

This work proposes for the first time the high-order counterpart of the quasi-Helmholtz projectors for the stabilization of the EFIE when using high-order basis functions. The contribution will first present a general definition of the Star

Manuscript received 29 August 2023; revised 13 February 2024; accepted 20 February 2024. Date of publication 1 March 2024; date of current version 9 April 2024. This work has received funding from the European Union's Horizon 2020 research and innovation programme under the Marie Skłodowska-Curie (grant agreement n° 955476, project COMPETE), from the European Research Council (ERC) under the European Union's Horizon 2020 research and innovation programme (grant agreement n° 724846, project 321). *(Corresponding author: Francesco P. Andriulli.)*

Johann Bourhis and Francesco P. Andriulli are with the Department of Electronics and Telecommunications, Politecnico di Torino, 10129 Turin, Italy (e-mail: francesco.andriulli@polito.it).

Adrien Merlini is with the Microwave Department, IMT Atlantique, 29238 Brest, France (e-mail: adrien.merlini@imt-atlantique.fr).

Color versions of one or more figures in this article are available at https://doi.org/10.1109/TAP.2024.3369752.

Digital Object Identifier 10.1109/TAP.2024.3369752

basis functions in high-order that encompasses several choices in terms of basis elements and testing in the charge space. The contribution will then show that the consequential definition of the quasi-Helmholtz projectors is not dependent on any of these specific choices. Finally, the new projectors will be used to regularize the EFIE discretized with high-order elements.

This article is organized as follows. In Section II, we set the background and the notations. In Section III, we extend the definition of the quasi-Helmholtz projectors to the high-order framework. We show their completeness to represent the Graglia–Wilton–Peterson (GWP) basis [5] and their uniqueness with respect to the choice of the Star basis, as well as their application to solve the low-frequency breakdown. In Section IV, we present the implementation details required to achieve effective algorithms. Finally, Section V provides numerical results which validate the preconditioning technique on relevant scenarios. The results of this work were presented in a conference contribution [19] that generalized the preliminary investigations in [20].

II. Background and Notations

This section will introduce the necessary background material and notations on integral equations and related high-order discretizations. The treatment will be brief and with the primary goal of setting the notations. The interested reader is referred to the more extensive treatments in [5], [21], [22], [23], and [7] and references therein.

Consider the scattering from a PEC object with boundary Γ residing in a homogeneous medium with wavenumber k and characteristic impedance η. The current $\boldsymbol{J}$ induced on Γ by an incident electric field $\boldsymbol{E}^{\mathrm{i}}$ can be obtained by solving the EFIE [2]

$$\mathcal{T}\boldsymbol{J} = -\widehat{\boldsymbol{n}} \times \frac{1}{\eta}\boldsymbol{E}^{\mathrm{i}} \tag{1}$$

with

$$\mathcal{T} = jk\,\mathcal{T}_s - \frac{1}{jk}\,\mathcal{T}_h \tag{2}$$

where the vector and scalar potentials are defined as

$$(\mathcal{T}_s\boldsymbol{J})(\boldsymbol{r}) = \widehat{\boldsymbol{n}} \times \int_\Gamma G(\boldsymbol{r},\boldsymbol{r}')\boldsymbol{J}(\boldsymbol{r}')\,\mathrm{d}S(\boldsymbol{r}') \tag{3}$$

$$(\mathcal{T}_h\boldsymbol{J})(\boldsymbol{r}) = \widehat{\boldsymbol{n}} \times \nabla_\Gamma \int_\Gamma G(\boldsymbol{r},\boldsymbol{r}')\nabla_\Gamma \cdot \boldsymbol{J}(\boldsymbol{r}')\,\mathrm{d}S(\boldsymbol{r}') \tag{4}$$

and where $\widehat{\boldsymbol{n}}$ is the outgoing normal vector from Γ, ∇_Γ is the surface nabla operator, and Green's kernel is

$$G(\boldsymbol{r},\boldsymbol{r}') = \frac{e^{-jk|\boldsymbol{r}-\boldsymbol{r}'|}}{4\pi|\boldsymbol{r}-\boldsymbol{r}'|}. \tag{5}$$

The solution $\boldsymbol{J}$ of (1) lives in the functional space $H_{\mathrm{div}}^{-1/2}(\Gamma)$, for which a well-suited arbitrary order discretization approach is given by Nédélec's mixed-order div-conforming spaces [22], [23]. These spaces can be generated by different sets of basis functions [5], [21], [24]. In the following, for fixing ideas, we will focus on the GWP basis function set, but our considerations and findings will also apply to several other bases. The pth order GWPs are defined as the product of the RWGs (zeroth-order GWPs) with order p shifted Silvester–Lagrange functions [5]. In what follows, we denote by $\{\boldsymbol{\psi}_n^{(p)}\}_{n=1}^{N_p}$ the set of GWP basis functions, where the total number of functions is

$$N_p = (p+1)E_{\mathrm{int}} + p(p+1)C \tag{6}$$

with E_{int} and C the numbers of internal edges and cells of the mesh, respectively. A detailed definition of these basis functions is omitted here for space limitation, but we refer the reader to [5] and [21].

Define by $\mathbb{P}(\Gamma, p)$ the space of divergence of GWP functions which is of dimension $M_p = C(p+1)(p+2)/2$ [14]. Let us consider a basis for the space by $\sigma_m^{(p)}/\mathcal{J}$ with $\mathcal{J}$ the Jacobian determinant of the mesh parametrization and

$$\sigma_m^{(p)}(\boldsymbol{r}) = \begin{cases} \widehat{\sigma}_{i(m)}^{(p)} \circ F_{K_m}^{-1}(\boldsymbol{r}), & \text{if } \boldsymbol{r} \in K_m \\ 0, & \text{elsewhere} \end{cases} \tag{7}$$

where K_m is the single cell on which $\sigma_m^{(p)}$ is not zero, $i(m)$ is its local index on the cell K_m, F_{K_m} is the local-to-global mapping of the cell K_m, and $\widehat{\sigma}_{i(m)}^{(p)}$ is a polynomial of degree p in the local coordinates. One possible choice for $\{\widehat{\sigma}_i^{(p)}\}$, $i = 1, \ldots, (p+1)(p+2)/2$, is an interpolatory polynomial basis, so that we have $(p+1)(p+2)/2$ interpolatory points $\widehat{\boldsymbol{r}}_j$ in the local coordinates and the same number of interpolatory polynomials such that

$$\widehat{\sigma}_i^{(p)}(\widehat{\boldsymbol{r}}_j) = \delta_{ij} \tag{8}$$

where δ_{ij} is the Kronecker symbol.

Because of charge neutrality, the total number of degrees of freedoms (DoFs) for the divergence space (charge DoFs) is $M_p - N_{\mathrm{bodies}}$ [14], where N_{bodies} is the number of separate connected bodies of the mesh. The GWP space can be decomposed as a combination of nonsolenoidal functions, corresponding to the charge DoFs, and a combination of solenoidal (divergence free) functions that complement the charge DoFs.

The GWP functions $\{\boldsymbol{\psi}_n^{(p)}\}$ can be used within a BEM strategy, by approximating the current in (1) as

$$\boldsymbol{J}(\boldsymbol{r}) \approx \sum_{n=1}^{N_p} j_n \boldsymbol{\psi}_n^{(p)}(\boldsymbol{r}) \tag{9}$$

and, after testing (1) with the rotated GWP elements $\{\widehat{\boldsymbol{n}} \times \boldsymbol{\psi}_n^{(p)}\}$, the EFIE yields a matrix system

$$\mathbf{T}\boldsymbol{j} = \boldsymbol{e} \tag{10}$$

with

$$\mathbf{T} = jk\,\mathbf{T}_s + \frac{1}{jk}\,\mathbf{T}_h \tag{11}$$

where

$$[\mathbf{T}_s]_{mn} = \int_{\Gamma\times\Gamma} G(\boldsymbol{r},\boldsymbol{r}')\boldsymbol{\psi}_n^{(p)}(\boldsymbol{r}') \cdot \boldsymbol{\psi}_m^{(p)}(\boldsymbol{r})\mathrm{d}S(\boldsymbol{r}')\mathrm{d}S(\boldsymbol{r}) \tag{12}$$

$$[\mathbf{T}_h]_{mn} = \int_{\Gamma\times\Gamma} G(\boldsymbol{r},\boldsymbol{r}')\nabla_\Gamma \cdot \boldsymbol{\psi}_n^{(p)}(\boldsymbol{r}') \nabla_\Gamma \cdot \boldsymbol{\psi}_m^{(p)}(\boldsymbol{r})\,\mathrm{d}S(\boldsymbol{r}')\mathrm{d}S(\boldsymbol{r}) \tag{13}$$

$$[\boldsymbol{e}]_m = -\frac{1}{\eta}\int_\Gamma \boldsymbol{E}^{\mathrm{i}}(\boldsymbol{r}) \cdot \boldsymbol{\psi}_m^{(p)}(\boldsymbol{r})\,\mathrm{d}S(\boldsymbol{r}). \tag{14}$$

At low frequency, the EFIE faces several numerical challenges. First, the EFIE linear system becomes increasingly ill-conditioned for decreasing frequencies due to frequency ill-scaling of vector and scalar potentials [9]. In particular

$$\lim_{k\to 0} \mathrm{cond}(\mathbf{T}) = \mathcal{O}\left(k^{-2}\right). \tag{15}$$

This ill-conditioning impacts the accuracy of the solution and increases the number of iterations required by iterative solvers. A second numerical challenge is related to the loss of significant digits in the context of finite precision computations when evaluating the right-hand side $\boldsymbol{e}$, the solution $\boldsymbol{j}$, and the radiated field [9].

Both effects are related to the quasi-Helmholtz decomposition of the current, because solenoidal and nonsolenoidal contributions in the EFIE system have different frequency behaviors. By decomposing the source and testing elements into their solenoidal and nonsolenoidal components, it is possible to properly rescale these contributions to cure both these issues. In the zeroth-order case, this strategy can be applied in a particularly effective way by leveraging quasi-Helmholtz projectors [9]. Differently from other quasi-Helmholtz decompositions such as Loop–Star/Tree and related approaches, this mathematical tool allows for the rescaling of scalar and vector potential without perturbing the other conditioning properties of the equation. The generalization of quasi-Helmholtz projector strategies to the high-order case, however, is far from trivial because of the need for a proper extension of the graph Laplacian matrices [9] to the high-order case. Such a generalization will be the subject of Section III.

III. High-Order Quasi-Helmholtz Projectors

In this section, we will define high-order quasi-Helmholtz projectors to address the above-described low-frequency limitations of the EFIE in the high-order case. From the zeroth-order case [9], we learn that primal projectors can be obtained from a properly chosen *Star matrix*. The problem is that a unique definition of a Star matrix in high-order can be challenging [14]. In this contribution, we will propose one approach to define a Star matrix that, indeed, does not lead to a unique definition. We will equally show in this article, however, that the corresponding Star (nonsolenoidal) projector will be invariant, regardless of the nonuniqueness of the Star definition we will adopt.

A. Construction of the High-Order Quasi-Helmholtz Projectors

Given the coefficients $\boldsymbol{j}$ of a function expressed as a linear combination of GWP functions, one could think of building a high-order Loop–Star decomposition in the form

$$\boldsymbol{j} = \boldsymbol{\Sigma}_p \boldsymbol{s} + \boldsymbol{\Lambda}_p \boldsymbol{l} + \mathbf{H}_p \boldsymbol{h}. \tag{16}$$

Similar to the zeroth-order case, $\boldsymbol{\Lambda}_p$ and $\mathbf{H}_p$ express the local-Loops-to-GWP and global-cycles-to-GWP change in bases, respectively [9]. In the following, we will not need an explicit definition of these two matrices and we will not discuss them further. We will only be using the fact that both $\boldsymbol{\Lambda}_p$ and $\mathbf{H}_p$ contain coefficient representations of solenoidal functions. For such a definition, however, the interested reader can refer to [14] and [15], where, unlike in our approach, explicit Loops coefficients are required. As pertains to $\boldsymbol{\Sigma}_p$, we will refer to this matrix as the high-order Star matrix, with an abuse of terminology stemming from the zeroth-order case. Consider now the injective linear function $\mathcal{L}$

$$\begin{aligned} \mathcal{L}\colon \mathbb{P}(\Gamma, p) &\longrightarrow \mathbb{R}^{M_p} \\ q(\boldsymbol{r}) &\longmapsto \mathcal{L}q \end{aligned} \tag{17}$$

with $\mathcal{L}_m q := [\mathcal{L}q]_m$. It should be noted that injectivity and linearity imply

$$\mathcal{L}q = 0 \iff q(\boldsymbol{r}) = 0 \quad \forall \boldsymbol{r} \in \Gamma. \tag{18}$$

Now we can propose the following general definition for $\boldsymbol{\Sigma}_p$:

$$\left[\boldsymbol{\Sigma}_p\right]_{i,j} = \left[\mathcal{L}\nabla_\Gamma \cdot \boldsymbol{\psi}_i^{(p)}\right]_j. \tag{19}$$

By the construction of $\boldsymbol{\Sigma}_p$ and because $\boldsymbol{\Lambda}_p$ and $\mathbf{H}_p$ describe solenoidal functions, we get

$$\boldsymbol{\Sigma}_p^T \boldsymbol{\Lambda}_p = \mathbf{0} \tag{20}$$

and

$$\boldsymbol{\Sigma}_p^T \mathbf{H}_p = \mathbf{0}. \tag{21}$$

The above conditions result in that all the coefficients of solenoidal functions are in the null space of $\boldsymbol{\Sigma}_p^T$. In addition, the converse statement, all the elements of the null space of $\boldsymbol{\Sigma}_p^T$ are coefficients of solenoidal functions, is true following from (18) and (19). Since the solenoidal subspace of the GWPs has a dimension $N_p - M_p + N_{\text{bodies}}$ [14], the null space of $\boldsymbol{\Sigma}_p^T$ has dimension $N_p - M_p + N_{\text{bodies}}$. As a consequence, the dimension of the range of $\boldsymbol{\Sigma}_p^T$, which is also the dimension of the range of $\boldsymbol{\Sigma}_p$, equals to $N_p - (N_p - M_p + N_{\text{bodies}}) = M_p - N_{\text{bodies}}$. This fact proves that $[\boldsymbol{\Sigma}_p, \boldsymbol{\Lambda}_p, \mathbf{H}_p]$, a rectangular matrix, has a rank equal to the number of basis functions N_p in (6). This shows that our definition of the high-order Stars produces a valid complement of the solenoidal subspaces as the columns of $[\boldsymbol{\Sigma}_p, \boldsymbol{\Lambda}_p, \mathbf{H}_p]$ are coefficient representations of functions that generate the entire GWP space.

We are now ready to define the quasi-Helmoltz projectors. In particular, mimicking the zeroth-order case, define

$$\mathbf{P}_p^{\Sigma} = \boldsymbol{\Sigma}_p \left(\boldsymbol{\Sigma}_p^T \boldsymbol{\Sigma}_p\right)^{+} \boldsymbol{\Sigma}_p^T \tag{22}$$

and

$$\mathbf{P}_p^{\Lambda H} = \mathbf{I} - \mathbf{P}_p^{\Sigma} \tag{23}$$

in which "+" is used to denote the Moore–Penrose pseudoinverse [25]. It should be noted that because of the orthogonality of the projectors, i.e.,

$$\mathbf{P}_p^{\Sigma}\mathbf{P}_p^{\Lambda H} = \mathbf{P}_p^{\Sigma}\left(\mathbf{I} - \mathbf{P}_p^{\Sigma}\right) = \mathbf{P}_p^{\Lambda H}\mathbf{P}_p^{\Sigma} = \mathbf{P}_p^{\Sigma} - \mathbf{P}_p^{\Sigma} = \mathbf{0} \tag{24}$$

and because of completeness of the decomposition, $\mathbf{P}_p^{\Lambda H}$ is the projector onto the solenoidal (local and global Loops) subspace.

From the generality of our definition of $\boldsymbol{\Sigma}_p$ in (19), one could think of obtaining a different set of projectors for each specific choice $\boldsymbol{\Sigma}_p$. We will now prove instead that the

high-order quasi-Helmholtz projectors, with our definition, are invariant under any particular choice of the high-order Star matrix. In particular

Proposition 1: Consider two different operators $\mathcal{L}$ and $\widetilde{\mathcal{L}}$ both satisfying definition and properties in (17) with associated matrices $\boldsymbol{\Sigma}_p$ and $\widetilde{\boldsymbol{\Sigma}}_p$, respectively, defined via (19), then there exists an invertible matrix $\mathbf{M}$ so that $\widetilde{\boldsymbol{\Sigma}}_p = \boldsymbol{\Sigma}_p\mathbf{M}$.

Proof: Consider an arbitrary basis $\{b_k\}_{k=1}^{M_p}$ of $\mathbb{P}(\Gamma, p)$. We can then express the divergence of each $\boldsymbol{\psi}_i^{(p)}(\boldsymbol{r})$ as

$$\nabla \cdot \boldsymbol{\psi}_i^{(p)}(\boldsymbol{r}) = \sum_{k=1}^{M_p} a_{ik} b_k(\boldsymbol{r}) \tag{25}$$

with a proper set of coefficients $\{a_{ik}\}_{k=1}^{M_p}$ for each $\boldsymbol{\psi}_i^{(p)}(\boldsymbol{r})$. Since both $\boldsymbol{\Sigma}_p$ and $\widetilde{\boldsymbol{\Sigma}}_p$ are defined on the same GWP set $\boldsymbol{\psi}_i^{(p)}(\boldsymbol{r})$ and assuming the same ordering of the basis functions in both cases, from (25) we have

$$\boldsymbol{\Sigma}_p = \mathbf{AL} \quad \text{and } \widetilde{\boldsymbol{\Sigma}}_p = \mathbf{A}\widetilde{\mathbf{L}} \tag{26}$$

with $[\mathbf{A}]_{ik} = a_{ik}$, $[\mathbf{L}]_{kj} = \mathcal{L}_j b_k$, and $[\widetilde{\mathbf{L}}]_{kj} = \widetilde{\mathcal{L}}_j b_k$.

Using the definition, linearity, and injectivity of $\mathcal{L}$, together with the completeness of the basis $\{b_k\}_{k=1}^{M_p}$, we obtain

$$\begin{aligned} \mathbf{L}^T\boldsymbol{x} = \mathbf{0} &\Rightarrow \sum_{k=1}^{M_p} (\mathcal{L}_m b_k) x_k = 0 \quad \forall m \\ &\Rightarrow \mathcal{L}_m\left(\sum_{k=1}^{M_p} x_k b_k\right) = 0 \quad \forall m \\ &\Rightarrow \sum_{k=1}^{M_p} x_k b_k = 0 \Rightarrow \boldsymbol{x} = \mathbf{0} \end{aligned} \tag{27}$$

which, with linearity, establishes the invertibility of $\mathbf{L}$. The same strategy shows the invertibility of $\widetilde{\mathbf{L}}$. We now have

$$\mathbf{A} = \mathbf{A} \Rightarrow \mathbf{A}\widetilde{\mathbf{L}}\widetilde{\mathbf{L}}^{-1} = \mathbf{A}\mathbf{L}\mathbf{L}^{-1} \Rightarrow \widetilde{\boldsymbol{\Sigma}}_p\widetilde{\mathbf{L}}^{-1} = \boldsymbol{\Sigma}_p\mathbf{L}^{-1} \tag{28}$$

from which we obtain the looked for relationship

$$\widetilde{\boldsymbol{\Sigma}}_p = \boldsymbol{\Sigma}_p\mathbf{M} \tag{29}$$

with $\mathbf{M} = \mathbf{L}^{-1}\widetilde{\mathbf{L}}$, an invertible matrix. □

The well-posedness of the definition of the projectors in (22) and (23) now follows. In particular

Corollary 1: The quasi-Helmholtz projectors are invariant on any specific choice of a high-order Star matrix satisfying (19).

Proof: Given two matrices as above, we have from the previous proposition that $\widetilde{\boldsymbol{\Sigma}}_p = \boldsymbol{\Sigma}_p\mathbf{M}$ with $\mathbf{M}$ unique and invertible. First note that, letting

$$\boldsymbol{\Sigma}_p = \mathbf{USV}^T \tag{30}$$

be the reduced singular value decomposition (SVD) of $\boldsymbol{\Sigma}$ (i.e., the SVD where $\mathbf{U}$ and $\mathbf{V}$ both are vertically rectangular and column full rank), then

$$\mathbf{M}^T\boldsymbol{\Sigma}_p^T\boldsymbol{\Sigma}_p\mathbf{M} = \left(\mathbf{M}^T\mathbf{VS}^T\right)\left(\mathbf{SV}^T\mathbf{M}\right) \tag{31}$$

where the left matrix in parenthesis is a full column rank matrix and the right matrix in parenthesis is a full row rank matrix. Using the properties of pseudoinverses [25], we get

$$\left(\mathbf{M}^T\boldsymbol{\Sigma}_p^T\boldsymbol{\Sigma}_p\mathbf{M}\right)^+ = \left(\mathbf{SV}^T\mathbf{M}\right)^+\left(\mathbf{M}^T\mathbf{VS}^T\right)^+ \tag{32}$$

from which it follows that

$$\begin{aligned} \mathbf{P}_p^{\widetilde{\Sigma}} &= \widetilde{\boldsymbol{\Sigma}}_p\left(\widetilde{\boldsymbol{\Sigma}}_p^T\widetilde{\boldsymbol{\Sigma}}_p\right)^+\widetilde{\boldsymbol{\Sigma}}_p^T \\ &= \boldsymbol{\Sigma}_p\mathbf{M}\left(\mathbf{M}^T\boldsymbol{\Sigma}_p^T\boldsymbol{\Sigma}_p\mathbf{M}\right)^+\mathbf{M}^T\boldsymbol{\Sigma}_p^T \\ &= \mathbf{USV}^T\mathbf{M}\left(\mathbf{SV}^T\mathbf{M}\right)^+\left(\mathbf{M}^T\mathbf{VS}^T\right)^+\mathbf{M}^T\mathbf{VS}^T\mathbf{U}^T \\ &= \mathbf{UU}^T = \boldsymbol{\Sigma}_p\left(\boldsymbol{\Sigma}_p^T\boldsymbol{\Sigma}_p\right)^+\boldsymbol{\Sigma}_p^T = \mathbf{P}_p^{\Sigma}. \end{aligned} \tag{33}$$

The uniqueness of $\mathbf{P}_p^{\Sigma}$ combined with (23) directly implies that of $\mathbf{P}_p^{\Lambda H}$. □

B. Projector-Based Solution to the Low-Frequency Breakdown

To fix ideas and obtain an algorithm for the projectors, we propose to choose the following explicit definition of the Star matrix $\boldsymbol{\Sigma}_p$ [20]:

$$\left[\boldsymbol{\Sigma}_p^T\right]_{mn} = \int_\Gamma \sigma_m^{(p)}(\boldsymbol{r})\nabla_\Gamma \cdot \boldsymbol{\psi}_n^{(p)}(\boldsymbol{r})\,\mathrm{d}S(\boldsymbol{r}) \tag{34}$$

where the functions $\sigma_m^{(p)}$ are defined in (7) and (8). The reader should note that the rationale behind this choice is that this definition results in a standard Star matrix in the zeroth-order ($p = 0$) case and generalizes the concept for higher orders. Other choices, however, could have been made without modifying the final results, as proved above. Now, from (24), the high-order quasi-Helmholtz projectors satisfy

$$\mathbf{P}_p^{\Lambda H}\mathbf{T}_h = \mathbf{0} \quad \text{and } \mathbf{T}_h\mathbf{P}_p^{\Lambda H} = \mathbf{0} \tag{35}$$

which generalizes the analogous property valid in the zeroth-order case [9]. This allows to proceed with the same formal strategy developed for zeroth-order projectors that here will work for the high-order EFIE. Define the preconditioning matrix

$$\mathbf{P} = j\sqrt{k/C}\,\mathbf{P}_p^{\Sigma} + \sqrt{C/k}\,\mathbf{P}_p^{\Lambda H} \tag{36}$$

with the scaling factor

$$C = \sqrt{\frac{\|\mathbf{T}_h\|}{\left\|\mathbf{P}_p^{\Lambda H}\mathbf{T}_s\mathbf{P}_p^{\Lambda H}\right\|}}. \tag{37}$$

The preconditioned system reads

$$\mathbf{PTP}\boldsymbol{y} = \mathbf{P}\boldsymbol{e} \tag{38}$$

with

$$\boldsymbol{j} = \mathbf{P}\boldsymbol{y}. \tag{39}$$

The proof of low-frequency well-conditioning and stability of (38) is formally identical to the one for the zeroth-order case [9] and we omit it here for the sake of conciseness.

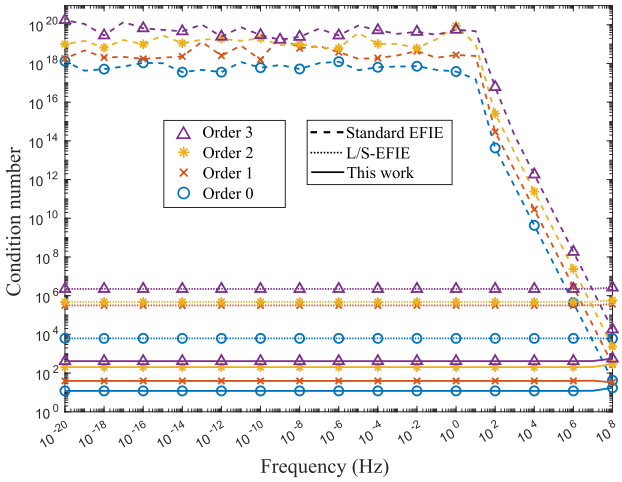

Fig. 1. Condition number of the system matrices in function of the frequency for order zero to three.

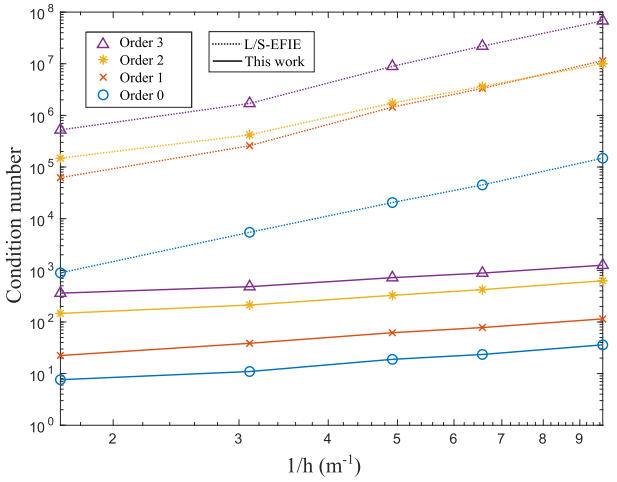

Fig. 2. Condition number of the system matrices in function of the inverse of the average cell diameter h and frequency of 1 Hz.

IV. Implementation-Related Details

In this section, we deal with implementation-related details that could be useful to the reader while implementing all the new techniques described here.

We assume that all the matrix–vector products are done in a quasi-linear number of operations, using a compression approach [26], [27] for the integral operators and a sparse algorithm for the Star matrices. Note that to match the computational complexity of fast matrix–vector product algorithms, the naive computation of the norms in (37) should be avoided and iterative approaches, such as power iterations [28], should be used instead. Moreover, the numerical (pseudo-)inversion of $\mathbf{\Sigma}_p^T\mathbf{\Sigma}_p$ in (22) has to be done iteratively whenever a product with the projectors is involved. As in the zeroth-order case, this matrix is similar to the one we get by discretizing the Laplacian equation with finite elements of order p. We can thus rely on algorithms tailored to solve such systems from other fields of applications [29]. In particular, multigrid algorithms have proven to be quite effective. Because there exists several variants of multigrids, one could use the p-multigrid versions [29], [30], [31] (tailored for high-order finite elements) but there are also robust implementations of the standard algebraic multigrid [32] generalized to different scenarios that are often easier to use in a black-box fashion.

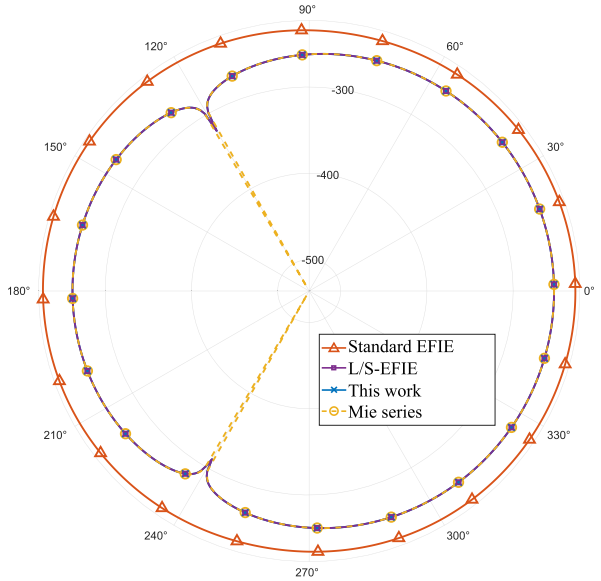

Fig. 3. RCS in dBsm at 100 Hz.

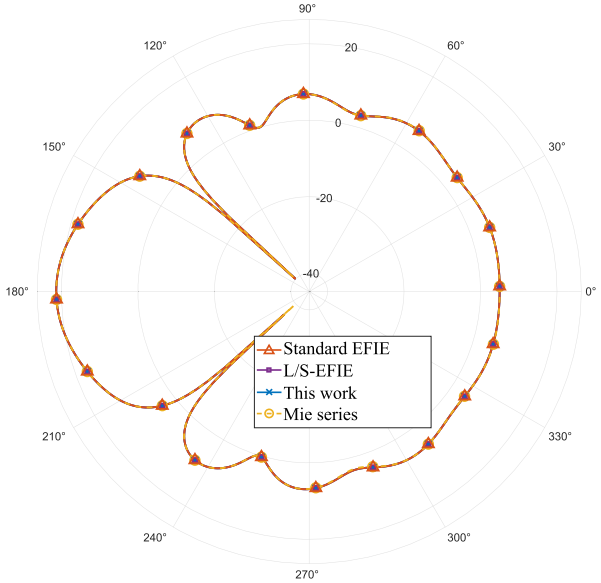

Fig. 4. RCS in dBsm at 3×10^8 Hz.

Finally, to maximize the effect of our regularization to all the frequencies, the computation of the projected EFIE has to be done carefully. For numerical purposes, the cancellations (35) have to be enforced explicitly in the computation of the preconditioned matrix [9], which reads

$$\mathbf{PTP} = jC\,\mathbf{P}_p^{\Lambda H}\mathbf{T}_s\mathbf{P}_p^{\Lambda H} + j/C\,\mathbf{T}_h - k\,\mathbf{P}_p^{\Lambda H}\mathbf{T}_s\mathbf{P}_p^{\Sigma} - k\,\mathbf{P}_p^{\Sigma}\mathbf{T}_s\mathbf{P}_p^{\Lambda H} - jk^2/C\,\mathbf{P}_p^{\Sigma}\mathbf{T}_s\mathbf{P}_p^{\Sigma}. \quad (40)$$

The loss of significant digits in the computation of the right-hand side also has to be avoided, as is well-known when dealing with very low-frequency numerical strategies [9]. In particular, the solenoidal and nonsolenoidal contributions of the right-hand side must be computed separately, and the static

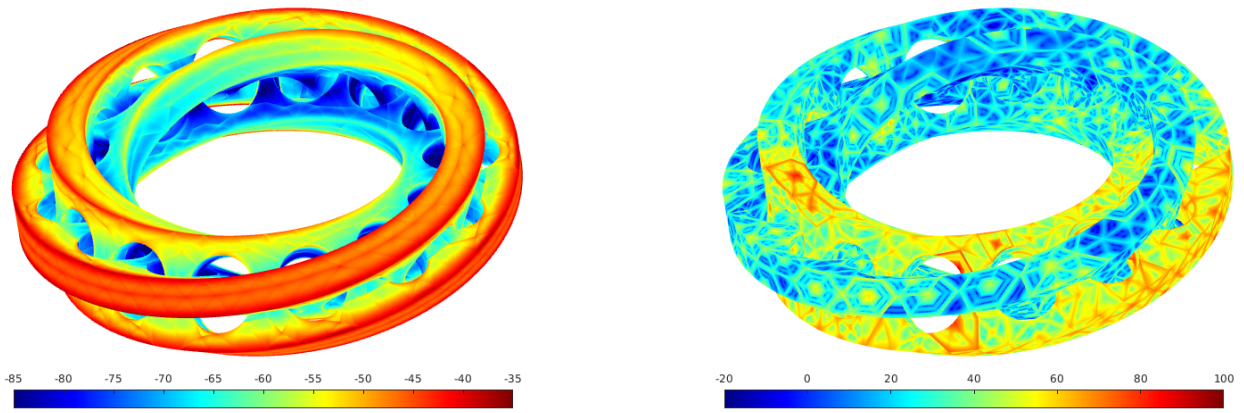

Fig. 5. Absolute value of the surface density current (in $\mathrm{dB_{A/m}}$) for the interlocked Möbius ring irradiated by a plane wave at 10 Hz, with preconditioning (left) and without (right).

part of the excitation source is subtracted when tested with the solenoidal functions [9], [11]. More explicitly, we write

$$\mathbf{P}\boldsymbol{e} = j\sqrt{k/C}\,\mathbf{P}_p^{\Sigma}\boldsymbol{e} + \sqrt{C/k}\,\mathbf{P}_p^{\Lambda H}\boldsymbol{e}_{\mathrm{sub}} \tag{41}$$

where $\boldsymbol{e}_{\mathrm{sub}}$ is the subtracted right-hand side [9]. Finally, the postprocessing computation of the electric field requires a similar treatment, using separately the solenoidal and non-solenoidal contributions of the solution

$$\boldsymbol{j}_{\mathrm{sol}} = \sqrt{C/k}\,\mathbf{P}_p^{\Lambda H}\boldsymbol{y} \quad \text{and} \quad \boldsymbol{j}_{\mathrm{nsol}} = j\sqrt{k/C}\,\mathbf{P}_p^{\Sigma}\boldsymbol{y} \tag{42}$$

and subtracting the static part of Green's kernel when integrating with the solenoidal contribution [9].

V. Numerical Validation

In this section, we give the numerical results that validate the use of the quasi-Helmholtz projectors by comparing it against the standard EFIE and against a standard quasi-Helmholtz decomposition. The quasi-Helmholtz decomposition we adopted for comparison is a generalization of the Loop/Star technique (L/S-EFIE) from the zeroth-order: the matrix $\mathbf{\Sigma}_p$ is used for generating the Stars and the Loops are computed as described in [14]. The meshes are generated from the software Gmsh that provides quadratic (curvilinear) triangles [33]. The singular integrals are computed using the singularity cancellation scheme described in [3] while near-singular and far interactions are computed with Gaussian quadratures. Moreover, because we are interested in studying the condition number of the underlying systems, the projectors need to be explicitly computed, which prevents the use of a fast strategy as described in Section IV. To this extent, we rely on a direct pseudoinversion of $\mathbf{\Sigma}^T\mathbf{\Sigma}$ based on the computation of its reduced SVD.

Our first validation is done over the unitary sphere for different frequencies. Fig. 1 shows the condition number of the system matrix for each different method as a function of frequency and for different orders. We observe that the condition number of the standard EFIE increases dramatically, as expected, while it remains constant for the standard Loop/Star technique and for the approach proposed here based on high-order quasi-Helmholtz projectors. For the latter case, however, the condition number is lower. This effect can be better understood from the test in Fig. 2 where the condition number is shown in function of the inverse mesh size. It is clear that differently from standard Loop/Star, the new projectors do not worsen the spectral behavior of the original EFIE generalizing what happens in the zeroth-order case [9]. The radar cross sections (RCSs) at 100 Hz and at 3×10^8 Hz are obtained in Figs. 3 and 4, respectively. This shows that the low-frequency breakdown, absent at higher frequencies, is instead corrupting the results at low frequency when no low-frequency treatment is used. At the same time, these results validate the stability of our scheme in a wide frequency range.

To test the performance of our scheme on a nonsimply connected geometry, we used the "two interlocked Möbius ring" structures, which form two separate objects with interlaced holes and handles. The rings are of radius 1 m and are discretized with 3780 cells and 5670 edges. In total, there are 72 global Loops associated with this topology. Fig. 5 shows the surface density current obtained by solving the EFIE with and without preconditioning at 10 Hz using basis functions of order two (39 690 unknowns). We get, without the need of detecting the global Loops, the same results with the quasi-Helmholtz projectors and the Loop/Star EFIE for which, however, the global Loops must be explicitly detected. It should also be noted that the accuracy is completely lost without preconditioning.

Our final validation test scenario is on the model of an airliner with 2-D apertures corresponding to the windows and the shell of the jet engine. The mesh contains 3942 cells and 5750 internal edges, and we use basis functions of order two (42 900 unknowns). In addition to show the relevance of our method to solve industrial scenarios, this example completes the numerical study with problems containing global Loops around apertures, which are of different kind than the harmonic Loops of the previous example. Fig. 6 shows the surface density current obtained by solving the EFIE with and without preconditioning at 1 Hz. As for the previous case, the quasi-Helmholtz projectors give an identical solution as the one obtained with Loop–Star decompositions (which however requires Loop detection), while the solution without preconditioning is completely jeopardized.

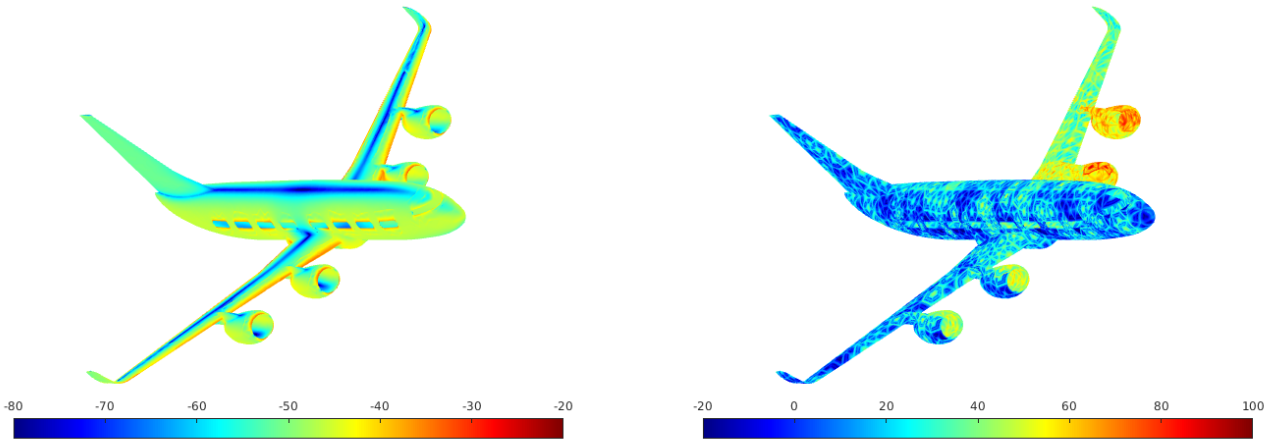

Fig. 6. Absolute value of the surface density current (in $\mathrm{dB_{A/m}}$) for the airliner irradiated by a plane wave at 1 Hz, with preconditioning (left) and without (right).

VI. Conclusion

In this work, we have extended the use of the quasi-Helmholtz projectors for stabilizing the EFIE when discretized with high-order basis functions. The new scheme is based on a generalized definition of Star matrix that is wide enough to encompass numerous relevant scenarios, including the use of GWP basis elements. The contribution has shown that this results into unique quasi-Helmholtz projectors irrespectively of the specific choice of Star matrix. The numerical results have shown the effectiveness of the new approach.

References

[1] W. C. Chew, E. Michielssen, J. Song, and J. Jin, *Fast and Efficient Algorithms in Computational Electromagnetics*. Norwood, MA, USA: Artech House, 2001.

[2] W. C. Gibson, *The Method of Moments in Electromagnetics*. Boca Raton, FL, USA: CRC Press, 2021.

[3] S. Sauter and C. Schwab, *Boundary Element Methods* (Springer Series in Computational Mathematics). Berlin, Germany: Springer, 2010.

[4] S. Rao, D. Wilton, and A. Glisson, "Electromagnetic scattering by surfaces of arbitrary shape," *IEEE Trans. Antennas Propag.*, vol. AP-30, no. 3, pp. 409–418, May 1982.

[5] R. D. Graglia, D. R. Wilton, and A. F. Peterson, "Higher order interpolatory vector bases for computational electromagnetics," *IEEE Trans. Antennas Propag.*, vol. 45, no. 3, pp. 329–342, Mar. 1997.

[6] R. D. Graglia and A. F. Peterson, *Higher-Order Techniques in Computational Electromagnetics*. Edison, NJ, USA: Scitech, Nov. 2015.

[7] M. Djordjevic and B. M. Notaros, "Double higher order method of moments for surface integral equation modeling of metallic and dielectric antennas and scatterers," *IEEE Trans. Antennas Propag.*, vol. 52, no. 8, pp. 2118–2129, Aug. 2004.

[8] A. F. Peterson and M. M. Bibby, "Error trends in higher-order discretizations of the EFIE and MFIE," in *Proc. IEEE Antennas Propag. Soc. Int. Symp.*, Jul. 2005, pp. 52–55.

[9] S. B. Adrian, A. Dély, D. Consoli, A. Merlini, and F. P. Andriulli, "Electromagnetic integral equations: Insights in conditioning and preconditioning," *IEEE Open J. Antennas Propag.*, vol. 2, pp. 1143–1174, 2021.

[10] G. Vecchi, "Loop-star decomposition of basis functions in the discretization of the EFIE," *IEEE Trans. Antennas Propag.*, vol. 47, no. 2, pp. 339–346, Feb. 1999.

[11] J.-S. Zhao and W. Cho Chew, "Integral equation solution of Maxwell's equations from zero frequency to microwave frequencies," *IEEE Trans. Antennas Propag.*, vol. 48, no. 10, pp. 1635–1645, Oct. 2000.

[12] J.-F. Lee, R. Lee, and R. J. Burkholder, "Loop star basis functions and a robust preconditioner for EFIE scattering problems," *IEEE Trans. Antennas Propag.*, vol. 51, no. 8, pp. 1855–1863, Aug. 2003.

[13] T. F. Eibert, "Iterative-solver convergence for loop-star and loop-tree decompositions in method-of-moments solutions of the electric-field integral equation," *IEEE Antennas Propag. Mag.*, vol. 46, no. 3, pp. 80–85, Jun. 2004.

[14] R. A. Wildman and D. S. Weile, "An accurate broad-band method of moments using higher order basis functions and tree-loop decomposition," *IEEE Trans. Antennas Propag.*, vol. 52, no. 11, pp. 3005–3011, Nov. 2004.

[15] F. Valdés, F. P. Andriulli, K. Cools, and E. Michielssen, "High-order div- and quasi curl-conforming basis functions for Calderón multiplicative preconditioning of the EFIE," *IEEE Trans. Antennas Propag.*, vol. 59, no. 4, pp. 1321–1337, Apr. 2011.

[16] C. L. Epstein and L. Greengard, "Debye sources and the numerical solution of the time harmonic Maxwell equations," *Commun. Pure Appl. Math.*, vol. 63, no. 4, pp. 413–463, Apr. 2010.

[17] X. Fu, J. Li, L. J. Jiang, and B. Shanker, "Generalized Debye sources-based EFIE solver on subdivision surfaces," *IEEE Trans. Antennas Propag.*, vol. 65, no. 10, pp. 5376–5386, Oct. 2017.

[18] Z.-G. Qian and W. C. Chew, "Enhanced A-EFIE with perturbation method," *IEEE Trans. Antennas Propag.*, vol. 58, no. 10, pp. 3256–3264, Oct. 2010.

[19] J. Bourhis, A. Merlini, and F. Andriulli, "High-order quasi-Helmholtz projectors: Definition, analyses, algorithms," in *Proc. 35th General Assembly Sci. Symp. Int. Union Radio Sci.*, 2023, pp. 1–7.

[20] A. Merlini, "Unified computational frameworks bridging low to high frequency simulations: Fast and high fidelity modelling from brain to radio-frequency scenarios," Ph.D. dissertation, Ecole Nationale Supérieure Mines-Télécom Atlantique, Brest, France, 2019.

[21] A. F. Peterson, "Mapped vector basis functions for electromagnetic integral equations," *Synth. Lectures Comput. Electromagn.*, vol. 1, no. 1, pp. 1–124, Jan. 2006.

[22] J. Nédélec, "Mixed finite elements in IR3," *Numerische Math.*, vol. 35, pp. 315–342, Sep. 1980.

[23] D. Boffi, F. Brezzi, and M. Fortin, *Mixed Finite Element Methods and Applications*. Berlin, Germany: Springer, 2013.

[24] B. M. Notaros, "Higher order frequency-domain computational electromagnetics," *IEEE Trans. Antennas Propag.*, vol. 56, no. 8, pp. 2251–2276, Aug. 2008.

[25] A. Ben-Israel and T. N. Greville, *Generalized Inverses: Theory and Applications*, vol. 15. Berlin, Germany: Springer, 2003.

[26] X.-M. Pan, L. Cai, and X.-Q. Sheng, "An efficient high order multilevel fast multipole algorithm for electromagnetic scattering analysis," *Prog. Electromagn. Res.*, vol. 126, pp. 85–100, 2012.

[27] S. Rjasanow and L. Weggler, "ACA accelerated high order BEM for Maxwell problems," *Comput. Mech.*, vol. 51, no. 4, pp. 431–441, Apr. 2013.

[28] G. W. Stewart, "A Krylov–Schur algorithm for large eigenproblems," *SIAM J. Matrix Anal. Appl.*, vol. 23, no. 3, pp. 601–614, Jan. 2002.

[29] B. Helenbrook, D. Mavriplis, and H. Atkins, "Analysis of 'p'-multigrid for continuous and discontinuous finite element discretizations," in *Proc. 16th AIAA Comput. Fluid Dyn. Conf.*, Jun. 2003, p. 3989.

[30] R. Tielen, M. Möller, D. Göddeke, and C. Vuik, "*p*-multigrid methods and their comparison to *h*-multigrid methods within isogeometric analysis," *Comput. Methods Appl. Mech. Eng.*, vol. 372, 2020, Art. no. 113347.
[31] I. Huismann, J. Stiller, and J. Fröhlich, "Scaling to the stars—A linearly scaling elliptic solver for p-multigrid," *J. Comput. Phys.*, vol. 398, Dec. 2019, Art. no. 108868.
[32] A. Napov and Y. Notay, "Algebraic multigrid for moderate order finite elements," *SIAM J. Sci. Comput.*, vol. 36, no. 4, pp. 1678–1707, Jan. 2014.
[33] C. Geuzaine and J.-F. Remacle, "Gmsh: A 3-D finite element mesh generator with built-in pre- and post-processing facilities," *Int. J. Numer. Methods Eng.*, vol. 79, pp. 1309–1331, Sep. 2009, doi: 10.1002/nme.2579.

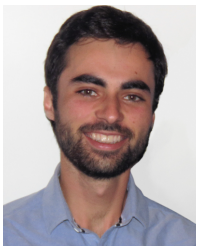

Johann Bourhis (Graduate Student Member, IEEE) received the M.Sc.Eng. degree in applied mathematics from the National Institute of Applied Sciences of Rennes (INSA Rennes), Rennes, France, in 2021, and the M.Sc. degree in scientific computing and modeling from the University of Rennes 1, Rennes, in 2021. He is currently pursuing the Ph.D. degree within a Marie Curie European Industrial Doctorate (EID) program in collaboration with the Politecnico di Torino, Turin, Italy, and Thales DMS, Élancourt, France.

Since 2021, he has been working as a Research Associate at the Politecnico di Torino, Turin, Italy. His research interests lie in the field of computational electromagnetics. His focus areas include preconditioning techniques and fast solvers for integral equations, particularly their adaptation to the framework of high-order boundary element methods.

Mr. Bourhis authored a paper that received an honorable mention at the IEEE Antennas and Propagation Symposium (IEEE AP-S) 2022. In addition, he was selected as a finalist for another paper in the Student Paper Competition at the URSI General Assembly and Scientific Symposium (URSI GASS) 2023, where he earned an additional Honorable Mention.

Adrien Merlini (Senior Member, IEEE) received the M.Sc.Eng. degree from the École Nationale Supérieure des Télécommunications de Bretagne (Télécom Bretagne), Brest, France, in 2015, and the Ph.D. degree from the École Nationale Supérieure Mines-Télécom Atlantique (IMT Atlantique), Brest, in 2019.

From 2018 to 2019, he was a visiting Ph.D. student with the Politecnico di Torino, Turin, Italy, where he then joined as a Research Associate. Since 2019, he has been an Associate Professor with the Microwave Department, IMT Atlantique. His research interests include preconditioning and acceleration of integral equation solvers for electromagnetic simulations and their application to brain imaging.

Dr. Merlini is a member of IEEE-HKN, the IEEE Antennas and Propagation Society, URSI France, and the Lab-STICC laboratory. He has received Young Scientist Awards at the URSI GASS 2020 and the EMTS 2023 meetings. He authored and coauthored award-winning papers, including the third place at the EMTS 2023 Best Paper Competition, the paper that received the 2022 ICEAA-IEEE APWC Best Paper Award, five papers that received honorable mentions (URSI/IEEE–APS 2021, 2022, and 2023), and three Best Paper Finalists (URSI GASS 2020 and URSI/IEEE–APS 2021 and 2022). He has been serving as an Associate Editor for *IEEE Antennas and Propagation Magazine*.

Francesco P. Andriulli (Fellow, IEEE) received the Laurea degree in electrical engineering from the Politecnico di Torino, Turin, Italy, in 2004, the M.Sc. degree in electrical engineering and computer science from the University of Illinois at Chicago, Chicago, IL, USA, in 2004, and the Ph.D. degree in electrical engineering from the University of Michigan at Ann Arbor, Ann Arbor, MI, USA, in 2008.

From 2008 to 2010, he was a Research Associate with the Politecnico di Torino, where he has been a Full Professor since 2017. From 2010 to 2017, he was an Associate Professor (from 2010 to 2014) and then a Full Professor with the École Nationale Supérieure Mines-Télécom Atlantique (IMT Atlantique, previously ENST Bretagne), Brest, France. His research interests are in computational electromagnetics with a focus on frequency- and time-domain integral equation solvers, well-conditioned formulations, fast solvers, low-frequency electromagnetic analyses, and modeling techniques for antennas, wireless components, microwave circuits, and biomedical applications with a special focus on brain imaging.

Prof. Andriulli is a member of Eta Kappa Nu, Tau Beta Pi, Phi Kappa Phi, and the International Union of Radio Science (URSI). He has received several best paper awards at conferences and symposia (URSI NA 2007, IEEE AP-S 2008, and ICEAA IEEE-APWC 2015) also in coauthorship with his students and collaborators (ICEAA IEEE-APWC 2021, EMTS 2016, URSI-DE Meeting 2014, and ICEAA 2009) with whom he also received a second prize conference paper (URSI GASS 2014), a third prize conference paper (IEEE–APS 2018), seven honorable mention conference papers (ICEAA 2011, URSI/IEEE–APS 2013, four in URSI/IEEE–APS 2022, and URSI/IEEE–APS 2023), and other three finalist conference papers (URSI/IEEE-APS 2012, URSI/IEEE-APS 2007, URSI/IEEE-APS 2006, and URSI/IEEE–APS 2022). He was a recipient of the 2014 IEEE AP-S Donald G. Dudley Jr. Undergraduate Teaching Award, the triennium 2014–2016 URSI Issac Koga Gold Medal, and the 2015 L.B. Felsen Award for excellence in electrodynamics. He has served as an Associate Editor for the IEEE TRANSACTIONS ON ANTENNAS AND PROPAGATION, IEEE ANTENNAS AND WIRELESS PROPAGATION LETTERS, and IEEE ACCESS and *IET Microwaves, Antennas and Propagation* (IET-MAP). He serves as a Track Editor for the IEEE TRANSACTIONS ON ANTENNAS AND PROPAGATION and an Associate Editor for *URSI Radio Science Letters*. He is the Editor-in-Chief of the *IEEE Antennas and Propagation Magazine*. He is the PI of the ERC Consolidator Grant: *321—From Cubic*^{3} *To*^{2} *Linear*^{1} *Complexity in Computational Electromagnetics.*

Open Access funding provided by 'Politecnico di Torino' within the CRUI CARE Agreement